$$
\left.
\begin{aligned}
f(i,j) &= f(x_i, y_j) \\
P(i,j) &= \sum_{l=1}^{\bar{N}} f(i,l)\bar{M}_j^l \\
Q(i,j) &= \sum_{k=1}^{N} f(k,j)M_i^k \\
R(i,j) &= \sum_{k=1}^{N}\sum_{l=1}^{\bar{N}} f(k,l)M_i^k \bar{M}_J^L
\end{aligned}
\right\} \quad i = 1 \ldots N,\ j = 1 \ldots \bar{N} \qquad (25.20)
$$

For $x < x_1$, $x > x_N$, $y < y_1$ or $y > y_{\bar{N}}$ we extrapolate by using respectively $S_{1,j}$, $S_{N-1,j}$, $S_{i,1}$, $S_{i,\bar{N}-1}$.

For one particular mesh the moments M_i^k and $\bar{M}_j^l$ of the cardinal splines have to be computed only once. The three sets of quantities P, Q, R have to be calculated once for each function f to be interpolated. (In our calculations we have six such functions: the dimensionless force and torque components). To any point (x,y) belongs a rectangle characterized by the numbers i and j, and the eight quantities A_i, B_i, C_i, D_i, $\bar{A}_j$, $\bar{B}_j$, $\bar{C}_j$, $\bar{D}_j$ can be computed for that point. Then S(x,y) as given by (25.19) yields the interpolated value for the function f at (x,y).

CHAPTER VI

WIND TUNNEL EXPERIMENTS.

§26 *Boomerang arms in uniform straight flow.*

The main part of this chapter is concerned with experiments on rotating boomerangs. This section, however, deals with a preliminary experiment in which lift and drag coefficients of boomerang arms in a uniform, straight air flow were measured. Boomerang arms, i.e. the wings forming part of a boomerang, in free flight operate at Reynolds numbers of the order of 10^5 or less. In this region the wing characteristics may seriously deviate from those at the higher Reynolds numbers associated with ordinary aircraft (see e.g. [Schmitz, 1957], [Muesmann, 1959], [Kraemer, 1961a]).

To investigate this matter with respect to our boomerang arms measurements were carried out with a small wind tunnel at the Twente University of Technology. Its wind speed could be varied between 0 and 30 m/s. (Degree of turbulence unknown.) The measuring cross section was square, having sides of 45.7 cm (18"). Lift and drag of wings were measured by means of a three-component spring balance mounted in one side wall of the tunnel. One end of the wing was attached to the spring balance in such a way that the wing's spanwise direction was horizontal, perpendicular to the airflow and halfway between the tunnel's bottom and ceiling. Four wings were made each of which occupied the full tunnel width, so that a two-dimensional flow (expectedly) would result. In addition six boomerang arms were cut off from actual boomerangs (which were known to fly well), and used in the experiment.

Here only part of the data shall be presented, but enough to provide a fairly representative picture of the lift and drag of boomerang arms in uniform straight flow at Re $\approx 4\times10^4$ to 10^5. It should be emphasized that the measurements were not of high precision. More extensive and accurate information (but not on hand-made boomerang arms) can be found in [Lippisch, 1951], [Schmitz, 1957, 1954], [Muesmann, 1959], [Kraemer,

1961a]. The data presented here are taken from 24 (out of 64) measuring series, and concern three of the six boomerang arms and all four "two-dimensional" wings. Their cross sections are shown in fig. 26.1.

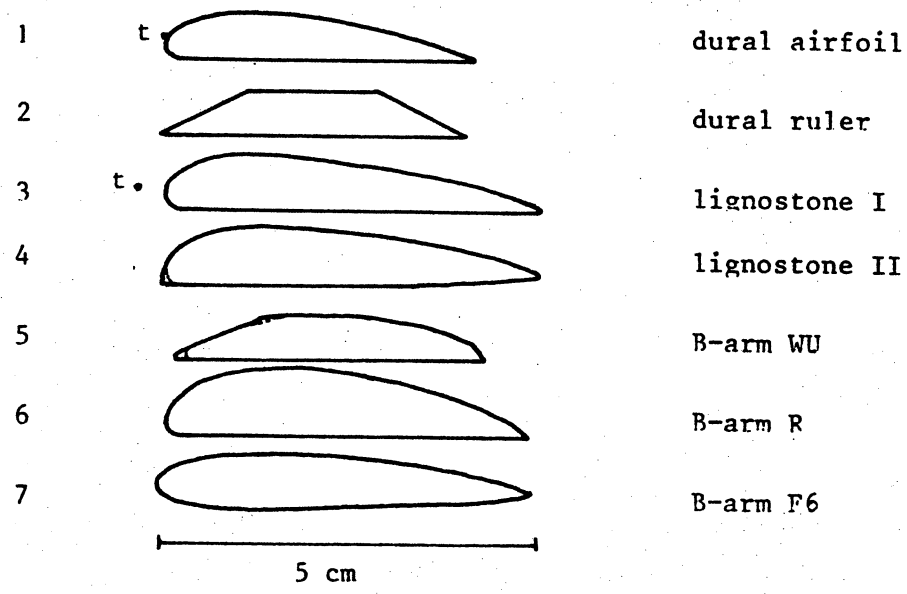

fig. 26.1. Cross sections of the wings used.
(t• = turbulence wire, ⌒ rounding off, in part of the measurements.)

wing	length l	AR	chord c	thickn. t	t/c	remarks
1 dural airfoil	45.4	∞	4.04	0.62	.154	also with turbulence wire
2 dural ruler	45.4	∞	3.97	0.57	.144	
3 lignostone I	45.4	∞	4.92	0.77	.157	also with turbulence wire
4 lignostone II	45.3	∞	4.88	0.76	.156	also rounded
5 B-arm WU	28.6	15	3.86	0.61	.158	also rounded
6 B-arm R	26.6	12	4.7	0.94	.200	
7 B-arm F6	25.6	10	4.9	0.72	.147	

table 26.1. Some dimensions (cm) of the wings used.

Table 26.1 lists some of the dimensions of the wings used. Boomerang arms R and F6 are tapered, and for these the chord and thickness in the middle are listed. The aspect ratio for the arms is defined as:

$$AR = \frac{2l^2}{s} \tag{26.1}$$

where l = spanwise length, s = wing area. The factor 2 is due to the mirror effect of the tunnel wall. For the four "two-dimensional" wings we take AR = ∞. The Reynolds number is defined as:

$$Re = \frac{Vc}{\nu} \tag{26.2}$$

where V = air velocity, ν = kinematic viscosity of air, c = chordlength as listed in table 26.1. Theoretically an elliptic spanwise lift distribution would give rise to an induced drag coefficient (see e.g. [von Mises, 1959]):

$$C_D = \frac{C_L^2}{\pi AR} \tag{26.3}$$

The corresponding parabolic curves are drawn as thin lines in fig. 26.3A, B,C. Figures 26.2A,B,C,D and 26.3A,B,C show experimental polar curves i.e. C_D, C_L graphs. The numbers in the graphs denote the angles of incidence, which, in this section, are the angles between the undisturbed airflow and the flat(test) part of the underside of the considered wing. Let us consider the experimental data wing for wing.

1. Dural airfoil: fig. 26.2A, fig. 26.3D.
This wing is milled from duraluminium. It has a smooth, airfoil-shaped profile. Similar wings were used in the experiments under water, described in §17 and §18. Comparison of the curve O Re = 77000 (V = 28.7 m/s) with the curve ⊕ Re = 44000 (V = 16.4 m/s) shows the dependence on Re of both C_L and C_D. The favourable influence of a turbulence wire at Re = 44000 (V = 16.4 m/s) is evident from a comparison between the curves ⊕ without wire and ▲ with wire. The wire consisted of a piece of 0.05 cm thick cotton string glued to the wing's nose at both ends. Its position was influenced by the airflow, especially in the middle of the wing. As the wire touched the wing's nose it should be considered as a trip wire, see [Kraemer, 1961b]. Finally the curve ◯ Re = 77000 (V = 28.6 m/s)

gives data for the reversed profile. Polar curves at Re = 81000 (not shown) are essentially the same as those at Re = 77000 (0,◯). Fig. 26.3D shows a remarkable hysteresis phenomenon. C_L and C_D are plotted as functions of Re (or V) at a constant angle of incidence of 5°. For Re > 65000: $C_L \approx 1.0$ and $C_D \approx 0.05$, whereas for Re < 53000: $C_L \approx 0.5$ and $C_D \approx 0.1$. For 53000 < Re < 65000 the lift and drag coefficients depend on whether the situation was reached from the super- or from the subcritical state (see further down in this section).

2. Dural ruler: fig. 26.2C.
This wing was milled from duraluminium. It has a trapezium-shaped cross section with sharp edges, and front-rear symmetry. The trapezium's sharp angles equal 27.4°. The lift and drag characteristics are not significantly different at Re = 79000 (V = 29.8 m/s): O and Re = 44000 (V = 16.5 m/s): ⊕. C_D increases suddenly above 7½° angle of incidence, and again above 15°.

3. Lignostone I, fig. 26.2B.
This wing was hand-made from lignostone, a kind of impregnated, compressed beech ply. It has a flat underside. Its upper side was filed into shape and sanded smooth. The measurements were done without and with turbulence wire. In the latter case the wire consisted of a 0.05 cm (= 0.01 chord) thick piece of cotton string stretched in front of the wing's leading edge, parallel to it, at a distance of 0.3 cm (= 0.06 chord). The wire was fastened to the wing by means of two screws near the wing's ends. Without wire there is a slight dependence on Re: compare curve O at Re = 97000 (V = 29.6 m/s) with curve ⊕ at Re = 55000 (V = 16.7 m/s). With wire the Re dependence is restricted to angles of incidence higher than 10°: compare curve Δ at Re = 96000 (V = 29.2 m/s) with curve ▲ at Re = 54000 (V = 16.3 m/s). The influence of the turbulence wire is very pronounced: compare Δ with O resp. ▲ with ⊕. Stall is postponed by the wire from 5° to 12½° resp. from 2½° to 10°, and the maximum C_L is increased from 1.0 to 1.3 resp. from 0.8 to 1.2. At Re = 96000 strong flutter occurred for angles of incidence near 15°. The curve ⊕ at Re = 55000 (V = 16.7 m/s) gives data for the reversed profile.

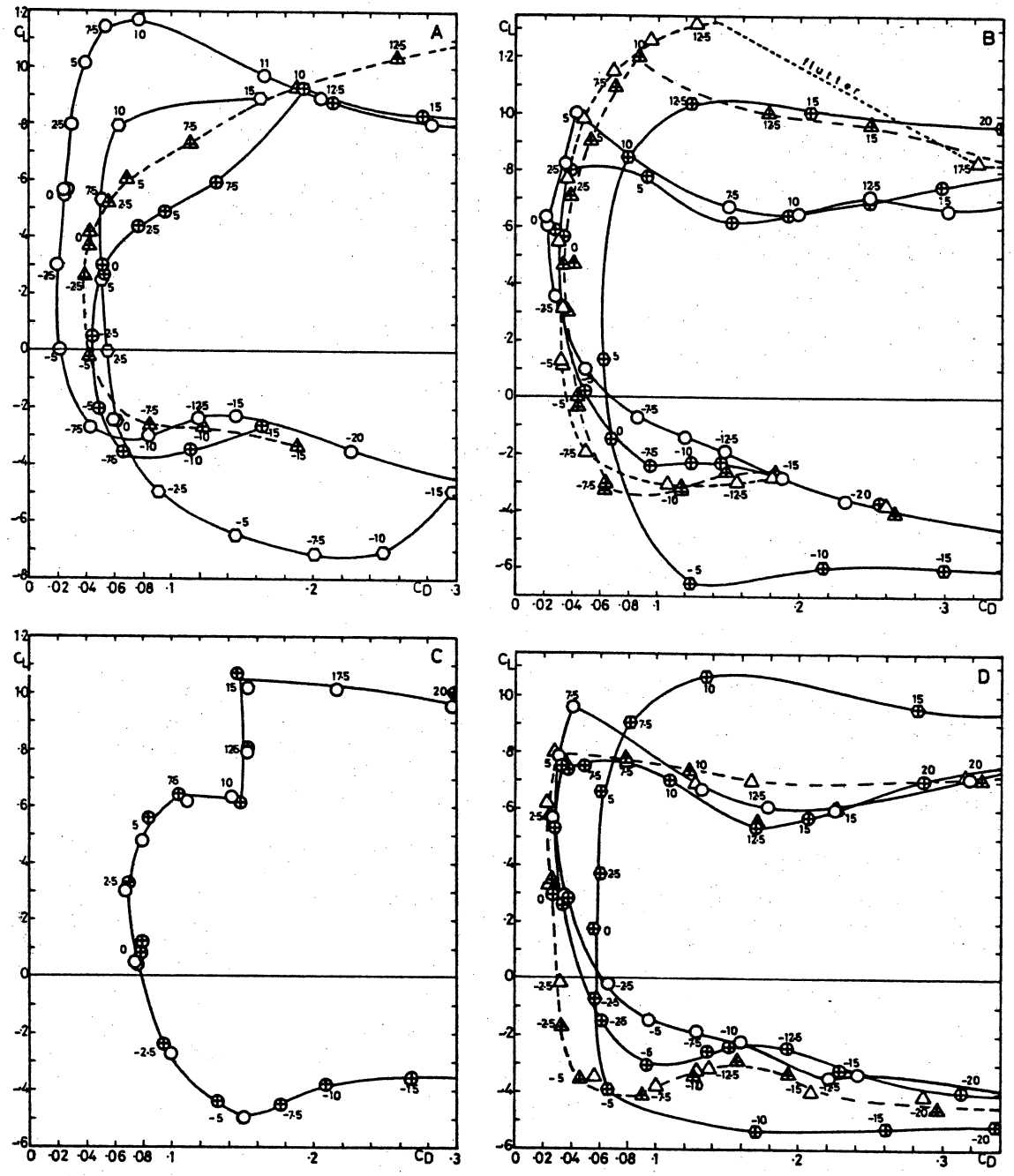

fig. 26.2. Experimental polar curves for 4 two-dimensional wings.
A. dural airfoil, O normal Re = 77000, ⊕ normal Re = 44000, ▲ with turbulence wire Re = 44000, ⬡ reversed Re = 77000.
B. lignostone I, O normal Re = 97000, ⊕ normal Re = 55000, Δ with turbulence wire Re = 96000, ▲ with turbulence wire Re = 54000, ⨁ reversed Re = 55000.
C. dural ruler, O Re = 79000, ⊕ Re = 44000.
D. lignostone II, O normal Re = 98000, ⊕ normal Re = 53000, Δ rounded Re = 96000, ▲ rounded Re = 53000, ⨁ reversed Re = 53000.
Numbers with the experimental points denote the angles of incidence.

4. Lignostone II, fig. 26.2D.
This wing was hand-made from lignostone. The main difference from lignostone I is that the underside of lignostone II is not entirely flat, but somewhat curved upward near de trailing edge. The flat part meets the nose of the profile at a right angle with a sharp edge. In addition measurements were made in which this edge was rounded off. The effects of this rounding on C_L and C_D are negligible, except at negative angles of incidence where it is favourable: compare curve O at Re = 98000 (V = 30.0 m/s) resp. ⊕ at Re = 54000 (V = 16.7 m/s) with Δ at Re = 96000 (V = 29.4 m/s) resp. ▲ at Re = 53000 (V = 16.4 m/s). The polar curves, including ⊕ at Re = 54000 (V = 16.7 m/s) for the reversed profile, resemble the corresponding curves (O,⊕,⊕ for lignostone I. The curve for the reversed profile at Re = 98000 (not shown) is not different from that at Re = 54000 (⊕).

5. B-arm WU, fig. 26.3B.
This wing was cut from a nylon boomerang, which is commercially made and available in Germany under the name "Comeback" (see fig. 28.1). Curiously, the profile has a sharp leading edge, a less sharp trailing edge and a kink in its upper side. Its underside is nearly flat. According to the designer, Mr. W. Urban (personal communication, 1970), these features were not based on aerodynamic considerations, although he had made boomerang flight trials with various wing profiles. Rounding off the leading edge and the kink has an adverse effect on C_L and C_D for angles of incidence between 2½° and 10°: compare curve O at Re = 74000 (V = 29.2 m/s) with curve Δ for the rounded wing at Re = 76000 (V = 29.4 m/s). This effect is absent at Re = 42000 (not shown). Since rounding of the kink only has no significant effect either at Re = 76000 or at Re = 42000 (not shown), the effect should be mainly due to rounding of the leading edge. The reversed wing at Re = 76000 (V = 29.4 m/s), curve ○, has roughly the same characteristics as the normal wing, except for its angle of zero lift being -2½° instead of 0°. The rounding has no substantial effect on the characteristics of the reversed profile (not shown). The polar curves of the not-rounded wing at Re = 42000 (not shown) do not differ much from those at Re = 76000 (O,○).

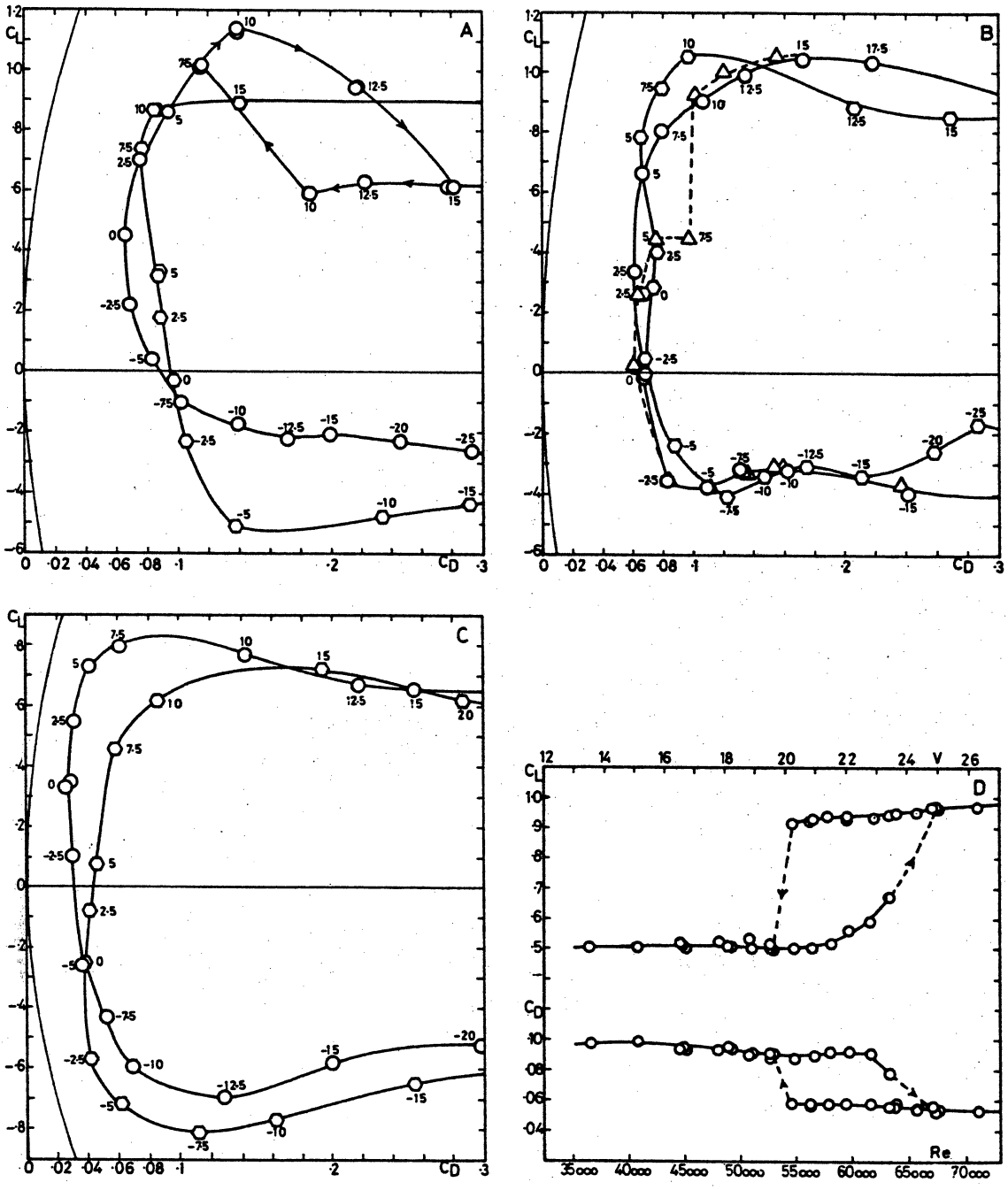

fig. 26.3. Experimental polar curves for 3 boomerang arms.
A. B-arm R, O normal Re = 92000, ⬡ reversed Re = 92000.
B. B-arm WU, O normal Re = 74000, Δ rounded Re = 76000, ⬡ reversed Re = 74000.
C. B-arm F6, O normal Re = 96000, ⬡ reversed Re = 96000.
Numbers with the experimental points denote the angles of incidence.

D. dural airfoil, C_L and C_D vs. Re at constant angle of incidence 5°.

6. B-arm R, fig. 26.3A.
This wing was cut from a hand-made, painted, birch ply boomerang. The wing has a flat underside and is rather thick. The curve O at Re = 92000 (V = 29.2 m/s) exhibits a hysteresis for angles of incidence between 7½° and 15°. The reversed profile ar Re = 92000 (V = 29.2 m/s) is not much worse: curve ⬡.

7. B-arm F6, fig. 26.3C.
This wing was cut from a hand-made, painted, mahogany ply boomerang. The wing has a biconvex profile, its underside being less convex than its upper side. The polar curves at Re = 96000 (V = 29.4 m/s), both for the normal profile: O and for the reversed profile: ⬡, show a minimum C_D which is less than that for WU or R. The maximum C_L, however, is not high: 0.8. Two other boomerang arms having approximately the same profile were found to have similar polar curves (not shown).

The data represented here show the same peculiarities that are described more completely in the literature mentioned earlier in this section. The airflow around a wing appears to have two possible main states: a supercritical state at high Re and a subcritical state, with lower C_L and higher C_D, at low Re. The transition from the sub- to the supercritical state generally occurs at a somewhat higher Reynolds number than the reverse transition (hysteresis, see e.g. fig. 26.3D). Fig. 26.4 gives a schematic picture of the flow in both states. It is taken from

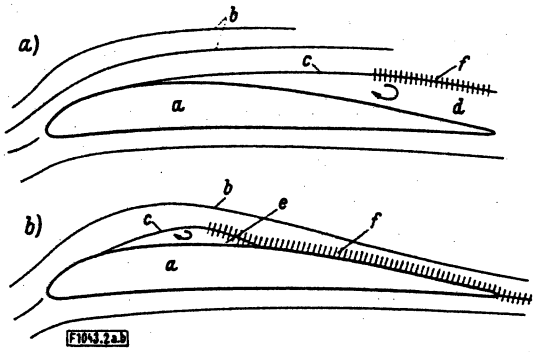

Fig. 26.4. Schematic picture of flow around airfoil (copied from [Kraemer, 1961a]). a) subcritical flow, b) supercritical flow. a = profile, b = streamlines, c = border stream line, d = dead water region, e = locally bounded dead water region ("Ablöseblase"), f = turbulent boundary layer.

[Kraemer, 1961] , together with the following clear description of the boundary layer phenomena:

Die sprunghafte Veränderung der Strömung und der aerodynamischen Beiwerte beim Durchlaufen der kritischen Reynoldszahl ist ein Grenzschichteffekt und hängt mit dem Umschlag der Grenzschicht von der laminaren in die turbulente Strömungsform zusammen. [...]
Ausgehend vom Staupunkt an der Flügelnase verläuft die Grenzschicht zunächst in jedem Fall laminar. Ist Re kleiner als die kritische Reynoldszahl, so bleibt die Grenzschicht auch hinter dem Druckminimum laminar und löst sich kurz danach von der Wand ab. Es entsteht ein Totwassergebiet, das sich bis hinter die Hinterkante erstreckt. Wird die kritische Reynoldszahl überschritten, so bildet sich im hinteren Teil der Flügel-Saugseite eine turbulente Grenzschicht; die Strömung kann nun (wenn der Anstellwinkel nicht zu gross ist) bis zur Hinterkante anliegen.
Der Grenzschichtumschlag von der laminaren in die turbulente Form vollzieht sich bei sehr grossen Reynoldszahlen in der Umgebung des Druckminimums in der anliegenden Grenzschicht. Ist jedoch die Reynoldszahl nur wenig grösser als die kritische Reynoldszahl, so schlägt die Strömung erst hinter der laminaren Ablösestelle am Rand einer "Ablöseblase" um, wie es Bild [26.4] schematisch andeutet. Die Turbulenz entsteht dabei in einigem Abstand von der Wand in der Totwassergrenze. Entscheidend für das Zustandekommen der überkritischen Strömung mit kleinem Widerstand und grossem Auftrieb ist, dass sich die turbulente Totwassergrenze wieder an die Wand anlegt. Auch im unterkritischen Fall wird die Totwassergrenze schliesslich turbulent, ohne sich jedoch wieder an die Wand anzulegen.
Die beim Überschreiten der kritischen Reynoldszahl (trotz des verhältnismässig grossen Reibungsbeiwerts der turbulenten Grenzschicht) gemessene Widerstandsabnahme rührt daher, dass der durch die Ablösung verursachte Druckwiderstand grösser als der Reibungswiderstand ist. Auch der Zusatzwiderstand von Rauhigkeiten und Störkörpern (z. B. "Turbulenzdraht") an oder vor der Nase spielt in der Regel keine Rolle, wenn dadurch bei vorgegebener kleiner Reynoldszahl noch überkritische Strömung (statt unterkritischer) erreicht werden kann. [Kraemer, 1961a, p. 34]

The data discussed in this section turn out to be interesting with regard to boomerangs in a rather unexpected way. If the measured lift and drag characteristics are used in our winglet model to compute the forces on *rotating* boomerangs, the axial (lift) force comes out too low for $\psi \gtrsim 10°$ (see §32). Similar deviations have been observed by Muesmann [1958] in the case of axial flow compressors at low Reynolds numbers.

§27 *The experimental setup.*

The following part of this chapter deals with an experiment in which forces were measured on rotating boomerangs placed in an airflow. Five different boomerangs were used (see fig. 29.1), the rotational velocity ω, the air speed V and the boomerang's angle of incidence ψ were varied, and the six force and torque components - averaged over time - acting on the boomerangs were determined. At the outset the plan was to carry out dynamic measurements, i.e. measurements of the instantaneous forces, or of the forces as functions of the boomerang's azimuthal angle. But after some consideration this plan was discarded, as enormous difficulties would have to be overcome, such as the elimination of vibrations. Although the experimentally determined time-averaged forces provide less information than the instantaneous forces, they still can be used as a basis for the calculation of boomerang flightpaths, and moreover, they can be compared to the corresponding quantities computed on basis of the theory outlined in the preceding chapters.

This section presents a description of the experimental setup shown in fig. 27.1. During the measurements a boomerang is attached to the end of the rotating shaft by means of a flat, V-shaped piece of duraluminium (see fig. 27.1b). The centre of mass of the boomerang including this V-piece is situated on the axis of the shaft, and the boomerang's principal axis of inertia coincides with the axis of rotation. The shaft consists of a hollow cylindrical aluminium tube, and is connected by means of two ball-bearings to a frame in which the motor drive is mounted. This frame is constructed from aluminium angle beams arranged in a compact tetrahedral form, so as to make it light and rigid. On the motor shaft a disk with slits is mounted which, together with a light and a photocel, serves to control the boomerang's rotational speed. Just as with the experiments in water, described in §17, this part of the apparatus is considered as one unit, B.

Unit B is connected to a second frame, C, by means of six elements, which measure the aerodynamic forces acting on unit B. (The inertial forces due to vibrations are expected to cancel after averaging with respect to time.) Frame C too has has a tetrahedral shape, it is